Trigonal Bipyramidal and Related Molecules of the Main Group Elements: Investigation of Apparent Exceptions to the VSEPR Model through the Analysis of the Laplacian of the Electron Density

Ronald J. Gillespie,* Ian Bytheway, Robert S. DeWitte, and Richard F. W. Bader

Department of Chemistry, McMaster University, Hamilton, Ontario L8S 4M1, Canada

*Received August 6, 1993**

Topological analyses of the charge density (ρ) and the Laplacian of the charge density ($\nabla^2\rho$) for molecules of the types AF_4E (A = P, S, Cl; E = a lone pair of electrons) and YSF_4 (Y = O, NH, CH_2) are presented. Examination of the relative sizes and shapes of bonding and nonbonding valence shell charge concentrations (VSCC's), which are made evident from the study of $\nabla^2\rho$, enables the geometrical features of these molecules to be understood and shows that they are in agreement with the concepts of the VSEPR model of molecular geometry. The ellipticity of a region of charge concentration is introduced as a measure of its shape, and its utility is demonstrated by the relationship between the geometry of the AF_4E molecules and the size and shape of the lone pair. Similarly, the shape of the double-bond domain, *i.e.*, its ellipticity, in the YSF_4 molecules is shown to be an important factor in the determination of their geometry. These molecules have been cited as exceptions to the VSEPR model because of the unexpected increase in the Y–S–F_{eq} angle in the series OSF_4, $HNSF_4$, and H_2CSF_4. Examination of the shape of Y–S bond electron density shows, however, that the observed bond angles are consistent with an increased spreading of the double-bond domain in the equatorial plane of the molecule. Examination of the electron density distribution of the Y–S bond gives useful information about its nature in these molecules, and the representation of Y–S bonds by Lewis structures is discussed.

Introduction

The success of the VSEPR model in accounting for the geometry of molecules is well documented[1,2] although there are some apparent exceptions to the model. It is the purpose of this and following papers to examine the charge density distribution in molecules which appear to be exceptions to the VSEPR model in order to determine reasons for its apparent failure. In this paper we analyze the charge density distribution in several AF_4E and YSF_4 molecules, some of which have geometries that do not appear to be in full accord with the predictions of the VSEPR model. In following papers we discuss the shapes of the calcium dihalides which are angular and not linear as predicted by the VSEPR model and also the shapes of some transition metal molecules for which it which has often been assumed that the VSEPR model does not hold.

We can think of the VSEPR model as giving a very approximate picture of the electron density distribution of a molecule in terms of localized electron pairs. The total electron density distribution in a molecule can be calculated with considerable accuracy by the Hartree–Fock method, but it gives no obvious evidence for the localized electron pair domains of the VSEPR model. It has, however, been shown that an analysis of the electron density distribution in terms of its Laplacian

$$\nabla^2\rho = \frac{\partial^2\rho}{\partial x^2} + \frac{\partial^2\rho}{\partial y^2} + \frac{\partial^2\rho}{\partial z^2}$$

reveals features of the electron density distribution that are not otherwise evident. In regions where the charge density is locally concentrated, $-\nabla^2\rho$ is positive and where the charge density is locally depleted $-\nabla^2\rho$ is negative.[3] An important property of $-\nabla^2\rho$, not evident in the charge density itself, is that for a free atom it shows spherical regions of charge concentration separated by regions of charge depletion corresponding to the shell structure of an atom.[4] The valence shell charge concentration of an atom in a molecule is not spherical but is distorted to give both maxima and minima that in almost all cases correspond in number and position to the localized electron pairs of the VSEPR model.[4]

One of the important features of the VSEPR model is its ability to account, in a qualitative way, for deviations from ideal geometries in terms of the relative sizes of the domains of localized electron pairs.[1,2] Although electron pairs are not in general as localized as assumed in the VSEPR model, the localized charge concentrations revealed by the Laplacian have properties that mimic closely those assumed for electron pair domains in the VSEPR model, thus giving physical (quantum mechanical) justification to the model.[3,4] By studying the charge concentrations revealed by the Laplacian of the electron density, we can expect to obtain a better understanding of molecular geometries which do not appear to be in accord with the VSEPR model. In this paper we show that by taking into account the relative shapes of the regions of charge concentration, as well as their location and relative size, we can understand in detail the geometry of some trigonal bipyramidal and related molecules.

In order to obtain the total electron density of the molecules described in this work the Hartree–Fock method, based on linear combinations of nuclear-centered basis functions (modified atomic orbitals), was used to calculate a set of molecular orbitals from which the state function and total electron density of each molecule were obtained. It should be emphasized that the use of such basis functions is only a convenience and that no fundamental significance can be attached to any particular orbital set of basis functions. Only the resulting state function and properties that can be derived from it, such as the electron density distribution, have a fundamental significance. The Schrödinger equation is not solved in order to obtain the wave function *per se*, but to obtain from this function the properties of the system—the expectation values of the observables. Among these is the electron

* Abstract published in *Advance ACS Abstracts,* April 1, 1994.

(1) Gillespie, R. J.; Hargittai, I. *The VSEPR Model of Molecular Geometry*; Allyn and Bacon: Boston, 1991; Prentice Hall International: London, 1991.

(2) Gillespie, R. J. *Chem. Soc. Rev.* **1992,** 59.

(3) Bader, R. F. W.; Gillespie, R. J.; MacDougall, P. J. *J. Am. Chem. Soc.* **1988,** *110,* 7329.

(4) Bader, R. F. W. *Atoms In Molecules: A Quantum Theory*; Oxford University Press: Oxford, U.K., 1991.

0020-1669/94/1333-2115$04.50/0

Table 1. Calculated Geometrical Data and Selected Atomic Properties for the AX_4E Series of Molecules[a]

	PF_4^- [b]	SF_4	ClF_4^+
$r(A-F_{eq})$/pm	160.3	153.5 [154.5]	152.9
$r(A-F_{ax})$/pm	174.1 [173]	164.0 [164.6]	159.0
$\angle F_{eq}-A-F_{eq}$/deg	99.8	102.5 [101.6]	109.2
$\angle F_{ax}-A-F_{ax}$/deg	168.3	170.7 [173.1]	170.2
$\angle F_{eq}-A-F_{ax}$/deg	86.2	87.1	87.2
$q(F_{eq})$[c]	−0.845	−0.708	−0.309
$q(F_{ax})$	−0.865	−0.696	−0.426
$q(A)$	2.414	2.805	2.469
ϵ_L[d]	0.524	0.411	0.293
$\nabla^2\rho$	−0.498	−1.058	−1.824

[a] Where available, observed values[9,10] are given in brackets. [b] Only the observed $P-F_{ax}$ bond length from ref 9 is shown here for comparison though it should be noted that the SCF-calculated results given there are almost identical to our results. [c] The population of an atom Ω in a molecule, $N(\Omega)$, is obtained by integration of ρ over the basin of the atom. The corresponding net charge $q(\Omega) = Z_\Omega - N(\Omega)$ where Z_Ω is the nuclear charge. [d] Values of ϵ_L and $\nabla^2\rho$ are for the nonbonded charge concentration on the central atom.

density, introduced by Schrödinger in the fourth of his classic papers on "wave mechanics".[5]

The electron density distribution is a measurable property of a molecule that can be determined experimentally by X-ray crystallography. The discussion in this and the following papers is therefore based on a measurable property of a molecule that is independent of any orbital model. It provides an alternative to orbital models for the discussion and interpretation of molecular shape. As no experimental measurements have been made of the electron density of the molecules discussed in this paper, our discussion is based on calculated electron density distributions.

It has been demonstrated[6] that the basis sets employed in this work yield densities with topological properties, together with those of its associated Laplacian distributions, that are independent of further improvements in the basis set or the introduction of electron correlation. The values of ρ and $\nabla^2\rho$ at the critical points, and the positions of these points, change by small amounts with such improvements, but the type and number of critical points and the properties they define, which are the subject of this paper, remain unchanged.

Methods

Calculation and Topological Analysis of the Charge Density and Its Laplacian. The wave functions for the molecules studied in this work, with the exception of CH_2SF_4, were obtained from HF6-311G**/HF6-311G** calculations performed using the Gaussian 90 software package.[7] In the case of CH_2SF_4, the calculation at this level of theory gave an extraneous local maximum in ρ along the S–C bond indicative of an insufficiently accurate description of the charge distribution. A calculation at the HF6-311++G(2d,2p)/HF6-311++G(2d,2p) level, however, gave the expected bond critical point between the sulfur and carbon atoms but did not otherwise change the electron density distribution significantly.

Atomic properties were calculated using the AIMPAC suite of programs.[8] Full geometry optimizations were employed to obtain the lowest energy trigonal bipyramidal geometries, whereas the square pyramidal geometries were calculated with the imposition of C_{4v} symmetry.

Table 2. Calculated Geometrical Data for the Square Pyramidal Isomers of PF_4^-, SF_4, ClF_4^+, and OSF_4

	PF_4^-	SF_4	ClF_4^+	OSF_4
$r(A-F)$/pm	167.6	159.6	157.3	156.3
$r(S-O)$/pm				138.6
$\angle E-A-F^a$/deg	111.85	110.23	108.05	108.88
$\nabla^2\rho^b$	−0.535	−1.134	−1.889	−1.000
Δ^c/kJ mol^{-1}	−48.242	−50.901	−22.890	−20.164

[a] The angle made by the basal fluorine atoms with the C_4 axis of the square pyramid. [b] The value of $\nabla^2\rho$ at the (3,−3) critical point corresponding to the lone-pair charge concentration on the central A atom. For the case of OSF_4 this value is for the double-bond domain belonging to sulfur. [c] $\Delta = E$(trigonal bipyramid) − E(square pyramid), *i.e.*, the difference in energy between the calculated trigonal bipyramidal and square pyramidal isomers for these molecules.

In the case of the $HNSF_4$ molecule, a starting geometry unrelated to that observed was used in order to find the optimum position for the hydrogen atom. It was found to occupy a position in the axial plane of the molecule, as in the observed geometry.

The shape of a charge concentration can be conveniently described in terms of its ellipticity. At a point of maximal charge concentration there are three negative curvatures (*i.e.*, three negative eigenvalues, λ_1^L, λ_2^L, and λ_3^L, of the Hessian of $\nabla^2\rho$), of which the ratio of the smallest two (λ_2^L and λ_3^L) describes the deviation of a region of charge concentration from cylindrical symmetry along the axis defined by the largest value, λ_1^L, which is always in the radial direction. The ellipticity of the Laplacian of the charge density, ϵ_L, describes the asymmetry of the charge concentration in the tangent plane and is defined as

$$\epsilon_L = \frac{\lambda_2^L}{\lambda_3^L} - 1$$

A value of unity for the ratio λ_2^L/λ_3^L indicates a charge concentration with cylindrical symmetry. The ellipticity of the charge density at a bond critical point (ϵ_ρ) is similarly defined in terms of the curvatures of ρ

$$\epsilon_\rho = \frac{\lambda_2^\rho}{\lambda_3^\rho} - 1$$

Results and Discussion

The AX_4E Molecules: PF_4^-, SF_4, ClF_4^+. The VSEPR model predicts that AX_4E molecules have a disphenoidal shape based on a trigonal bipyramidal arrangement of five electron-pair domains in the valence shell of A with the larger lone-pair domain in a less crowded equatorial position.[1,2] Because they are in more crowded positions, the axial bond domains are predicted to be smaller and farther from the nucleus than the equatorial bond domains so the axial bonds are predicted to be longer, weaker, and more polar than the equatorial bonds. Sulfur tetrafluoride has long been known to have a geometry in accord with these predictions, and very recently PF_4^- was also found to have the same shape.[9] The results of our calculations for these molecules together with the known experimental geometries are given in Tables 1 and 2. In each case, the trigonal bipyramidal geometry was found to be of lower energy than the square pyramidal geometry, in agreement with the experimental geometry and the VSEPR model. Calculated bond lengths and bond angles are in good agreement with the experimental geometry when known.

The VSEPR model predicts not only the general shape of the molecule but other details concerning bond lengths, angles, and polarities. These predictions may be summarized as follows:

(1) With decreasing electronegativity of the central atom, the bonding electron pair is expected to move away from the central

(5) Schrödinger, E. *Ann. Phys.* **1926**, *81*, 109.
(6) Gatti, C.; MacDougall, P. J.; Bader, R. F. W. *J. Chem. Phys.* **1988**, *88*, 3792.
(7) Frisch, M. J.; Head-Grodon, M.; Trucks, G. W.; Foresman, J. B.; Schlegel, H. B.; Rahavachari, K.; Robb, M.; Binkley, J. S.; Gonzalez, C.; Martin, D. J.; Kahn, L. R.; Stewart, J. J. P.; Topiol, S.; Pople, J. A. *Gaussian 90*, Revision F; Gaussian, Inc.: Pittsburgh, PA, 1990.
(8) Beigler-König, F. W.; Bader, R. F. W.; Tang, T.-H. *J. Comput. Chem.* **1982**, *3*, 317. Copies of the AIMPAC suite of programs are available upon request to Professor R. F. W. Bader by email: bader@mcmail.cis.mcmaster.ca.
(9) Christe, K. O.; Dixon, D. A.; Mercier, H. P. A.; Sanders, J. C. P.; Schrobilgen, G. J.; Wilson, W. W. *J. Am. Chem. Soc.*, in press.

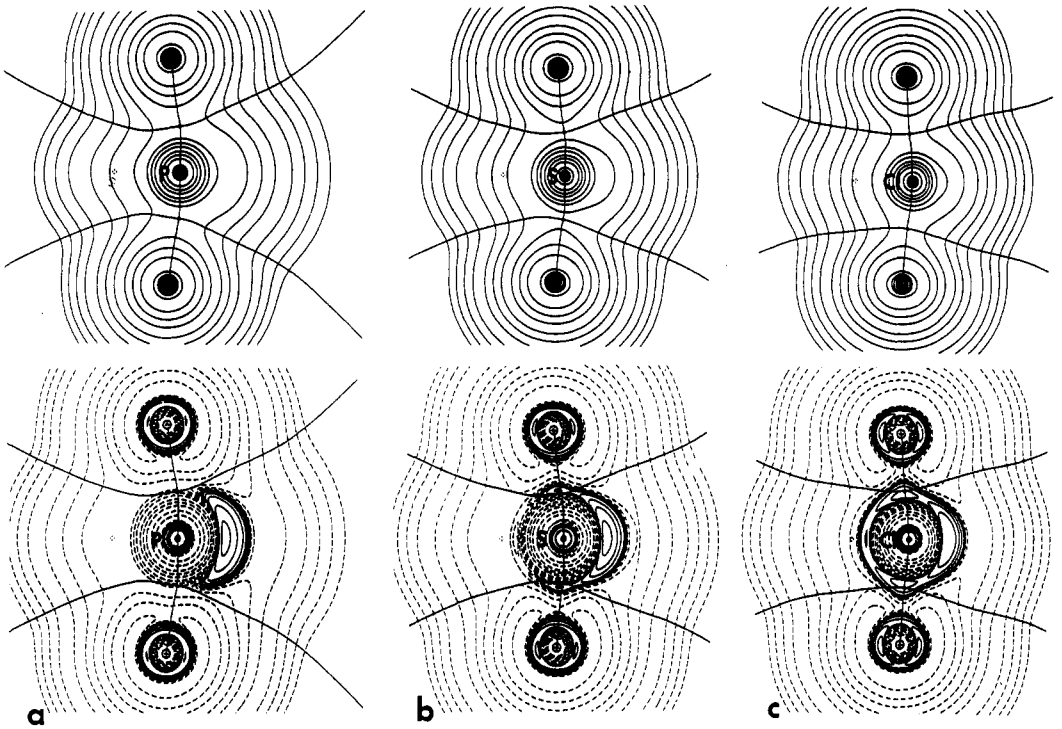

Figure 1. Contour maps of ρ (top) and $\nabla^2\rho$ (bottom) for the AF_4E molecules viewed in the plane containing both axial fluorine atoms, the central atom, and the nonbonded charge concentration: (a) PF_4^- (note the absence of charge concentration between the phosphorus and axial fluorine atoms); (b) SF_4 (bonded charge concentration between the sulfur and the axial fluorine atoms can be seen); (c) ClF_4^+ (increased bonded charge concentration is apparent, as is the decrease in the size and ellipticity of the region of nonbonded charge concentration). These and subsequent plots of ρ contours start at a value of 1×10^{-3} and increase in the order $2 \times 10^{\pm n}$, $4 \times 10^{\pm n}$, and $8 \times 10^{\pm n}$ for $n = 1$–3. For all plots of $\nabla^2\rho$ contours start at a value of 1×10^{-3} and change in steps of $\pm 2 \times 10^{\pm n}$, $\pm 4 \times 10^{\pm n}$, and $\pm 8 \times 10^{\pm n}$, for $n = 1$–3, with solid contour lines denoting negative values of $\nabla^2\rho$. Atomic boundaries and molecular graphs are overlayed in these and the following plots, bond critical points ((3,–1) critical points in ρ) are denoted by solid circles. Only nuclei other than fluorine have been labeled throughout this work.

atom and so the bonds are expected to increase in length and polarity in the series ClF_4^+, SF_4, PF_4^-. It can be seen in Table 1 that, in accordance with these predictions, the bond lengths and the charge on the fluorine atoms increase.

(2) The axial bond pairs are in more crowded positions than the equatorial bond pairs and are therefore farther from the nucleus than the equatorial pairs. The axial bonds are predicted to be longer and more polar than the equatorial bonds, as is shown by the bond lengths and charges given in Table 1.

(3) A lone-pair domain spreads out to occupy as much space as possible in the valence shell, pushing adjacent bond domains closer together. The larger the valence shell of the central atom, the more the lone-pair domain can spread out and the smaller the angle expected between the adjacent bonds. The valence shell increases in size in the series ClF_4^+, SF_4, PF_4^-, so the bond angles are expected to decrease correspondingly. Furthermore, it is expected that the lone pair will have a greater effect on the larger, and therefore more easily deformed, equatorial–equatorial bond angle than on the smaller, less easily deformed, equatorial–axial bond angles, as can be seen in Table 1.

(4) The prediction made in (3) implies that the lone pair is not axially symmetrical but is more spread out in the equatorial plane than in the axial plane. The shape of the lone-pair domain is of course not revealed by the experimental determination of the molecular geometry, but as we will see, it can be obtained from an analysis of the electron density distribution.

Plots of the Laplacian of the electron density for each of these three molecules are given in Figures 1 and 2. In each case, the analysis of the electron density is in accord with the concepts of the VSEPR model. For ClF_4^+ and SF_4 the Laplacian shows two axial and two equatorial charge concentrations and a lone-pair charge concentration in the valence shell of the central atom, but only the lone-pair charge concentration in PF_4^-. The size, shape, and positions of the charge concentrations revealed by the Laplacian of the electron density can now be related to the electron-pair domains of the VSEPR model and we see the following:

(1) The bonding charge concentrations decrease in size and move farther from the nucleus from ClF_4^+ to SF_4 and are absent in PF_4^- as the bonds become longer and more polar. We comment on the absence of the bonding charge concentrations in PF_4^- later.

(2) The axial charge concentrations are smaller and farther from the nucleus than the equatorial charge concentrations, and so the axial bonds are longer and more polar than the equatorial bonds.

(3) Figure 3 shows the Laplacian in a plane through the maximum of the lone-pair charge concentration and perpendicular to the C_2 axis of the molecule. The elliptical shapes of the lone-pair charge concentrations, which have their long axes in the equatorial plane, and their increase in size and ellipticity from Cl to P are clear in these plots. Quantitative information on the ellipticity is given by the values of ϵ_L in Table 1. The shapes of the lone-pair charge concentrations agree fully with the predictions of the VSEPR model.

The YSF_4 Molecules: OSF_4, $HNSF_4$, and H_2CSF_4. The results of our calculations for the molecules OSF_4, $HNSF_4$, and H_2CSF_4, along with the experimental geometries, are given in Table 3. The calculated geometries for OSF_4 and H_2CSF_4 are in good agreement with the experimental values,[10] while for $HNSF_4$ they compare favorably with the experimental values for $FNSF_4$ and CH_3SF_4.[11] The larger double-bond domain occupies a less crowded equatorial site in each case, and because of its larger size, the F–S–F angles are smaller than the ideal angles of 120 and 90°, respectively. With decreasing electronegativity of Y in the series Y = O, NH, CH_2, the double-bond domains are expected to occupy more space in the valence shell of sulfur, and the bond

(10) Oberhammer, H.; Boggs, J. E. *J. Mol. Struct.* **1979**, *56*, 107.
(11) Günther, H.; Oberhammer, H.; Mews, R.; Stahl, I. *Inorg. Chem.* **1982**, *21*, 1872.

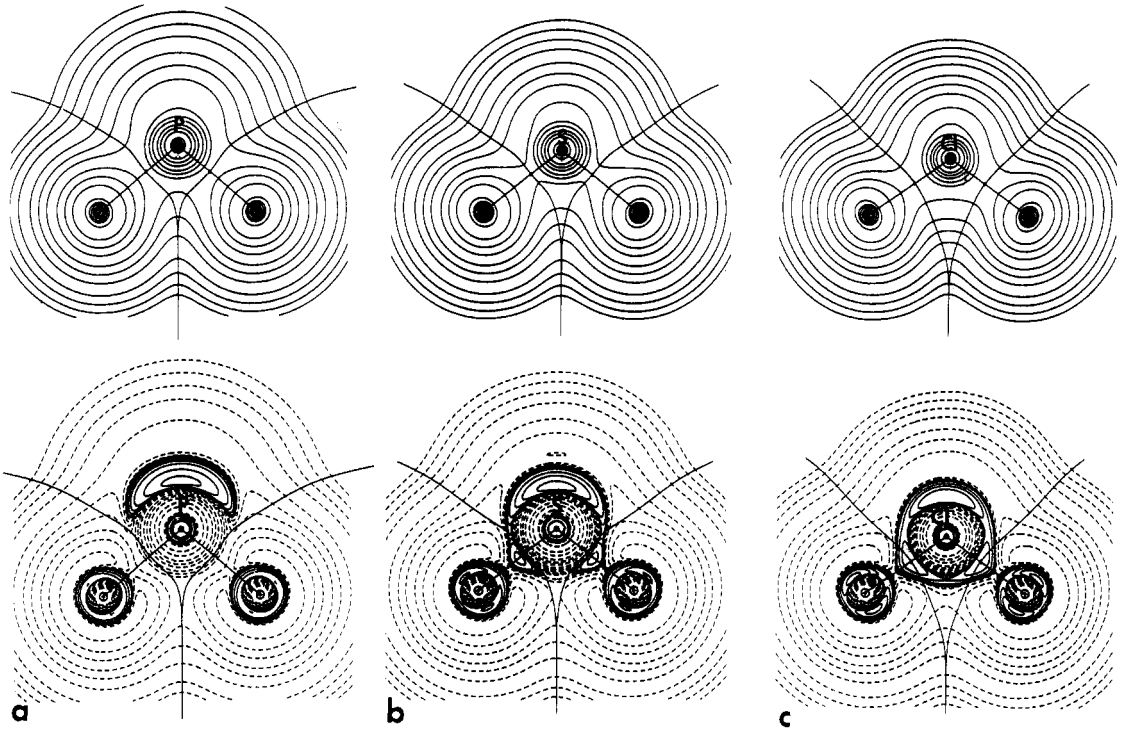

Figure 2. Contour maps of ρ (top) and $\nabla^2\rho$ (bottom) for the AF_4E molecules viewed in the plane containing both equatorial fluorine atoms, the central atom, and the nonbonded charge concentration: (a) PF_4^-; (b) SF_4; (c) ClF_4^+. The decrease in the amount of space occupied by the nonbonded charge concentration as the central atom changes from phosphorus to sulfur to chlorine is evident in these plots.

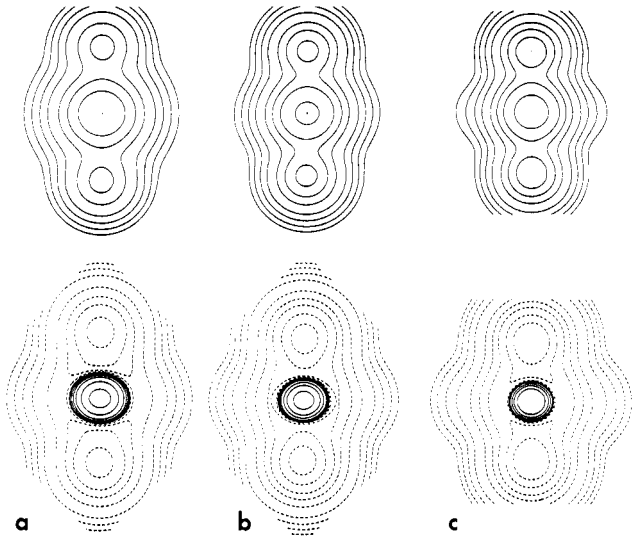

Figure 3. Contour maps of ρ (top) and $\nabla^2\rho$ (bottom) for the AF_4E molecules viewed in the plane obtained by taking a vertical slice through the nonbonded charge concentration maximum (for the both plots as there is no bond critical point to use for the map of ρ): (a) PF_4^-; (b) SF_4; (c) ClF_4^+. These plots demonstrate pictorially the notion of ellipticity and show how the regions of charge and charge concentration are distributed.

angles should therefore decrease correspondingly. The equatorial bond angle decreases as expected but the axial–equatorial and axial–axial bond angles *increase*. This apparently anomalous behavior can be understood, however, if the charge density distribution and its Laplacian are examined. The plots of the Laplacian of the charge density for OSF_4, $HNSF_4$, and H_2CSF_4 in Figures 4 and 5 show that the double-bond charge concentration has an ellipsoidal shape with its long axis in the equatorial plane. Plots of ρ through the bond critical point and of $\nabla^2\rho$ through the charge concentration maximum are given in Figure 6 and also show the elliptical shape of these regions. We see from Figure 6 and Table 3 that the ellipticity and magnitude of the double-bond charge concentration increases in the series Y = O, NH, CH_2 with decreasing electronegativity and decreasing charge on Y. As the ellipticity of the double bond increases and charge density moves from the axial plane to the equatorial plane, there is a corresponding increase in the axial angle.

Table 3. Calculated and Observed[10] Geometrical Data for the Trigonal Bipyramidal YSF_4 Molecules and Selected Atomic Properties[a]

	OSF_4	$HNSF_4$	H_2CSF_4
$r(S-F_{ax})$/pm	158.4	161.7	158.1
	[159.3]	[161.1]	[157.5]
		156.9	
		[156.9]	
$r(S-F_{eq})$/pm	152.8	153.8	153.5
	[153.5]	[155.0]	[159.5]
$r(S-Y)$/pm	139.2	147.3	156.2
	[140.6]	[146.1]	[155.0]
$\angle Y-A-F_{ax}$/deg	97.8	97.2	94.3
	[99.8]	[98.4]	[95.0]
		95.9	
		[94.6]	
$\angle Y-A-F_{eq}$/deg	124.0	128.0	130.9
	[122.9]	[128.7]	[131.8]
$\angle F_{eq}-A-F_{ax}$/deg	85.8	85.6	87.1
		87.0	
$q(F_{ax})$	−0.713	−0.717	−0.750
		−0.681	
$q(F_{eq})$	−0.695	−0.700	−0.732
$q(Y)$	−1.402	−1.661	−0.159
$q(H)$		0.457	0.0773
$q(S)$	4.211	4.003	2.959
$\epsilon_\rho{}^b$	0.152	0.547	0.977
$\rho_b{}^b$	0.342	0.323	0.287
$\epsilon_L{}^c$	1.380	2.124	6.559
$\nabla^2\rho^c$	−0.879	−1.052	−0.965

[a] Observed bond lengths and angles for OSF_4 and H_2CSF_4 are shown in brackets, while for $HNSF_4$ the bracketed values are for a previous calculation.[11] Two types of axial fluorine atom are present in the $HNSF_4$ molecule, the first for the fluorine closest to the hydrogen atom. [b] These values are for the value of ρ at the (3,−1) critical point (*i.e.*, the bond critical point) along the S–Y bond. [c] These values are for the (3,−3) critical point in $\nabla^2\rho$, corresponding to the charge concentration maximum in the valence shell of sulfur along the S–Y bond.

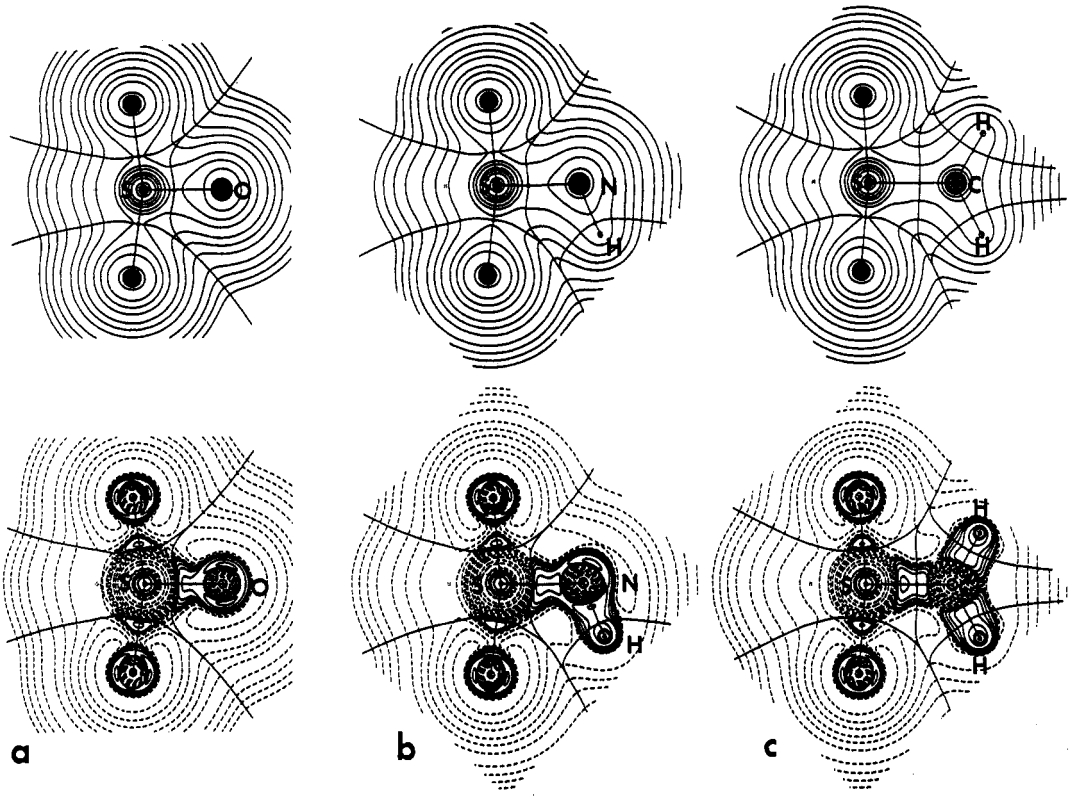

Figure 4. Contour maps of ρ (top) and $\nabla^2\rho$ (bottom) for the YSF_4 molecules viewed in the plane containing the axial fluorine, central, and doubly-bonded atoms: (a) OSF_4; (b) $HNSF_4$; (c) H_2CSF_4.

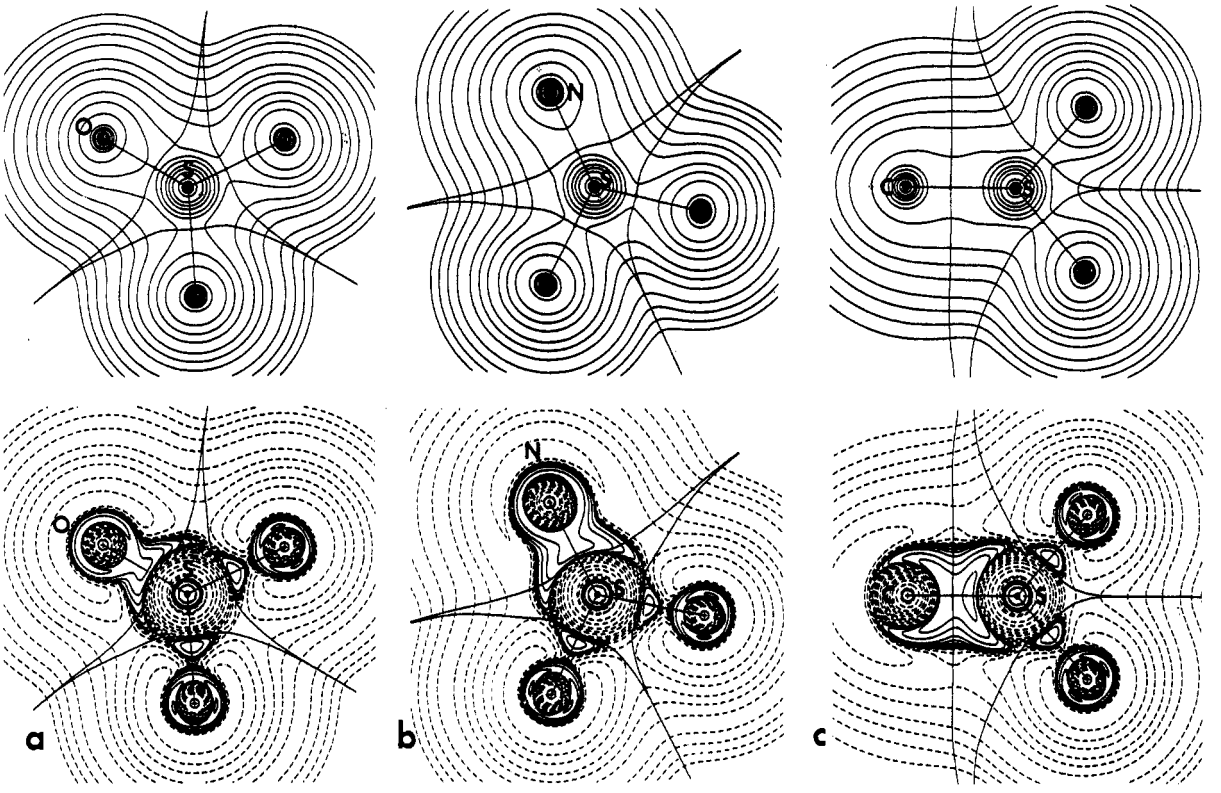

Figure 5. Contour maps of ρ (top) and $\nabla^2\rho$ (bottom) for the YSF_4 molecules viewed in the plane containing the equatorial fluorine, central, and doubly-bonded atoms: (a) OSF_4; (b) $HNSF_4$; (c) H_2CSF_4. The region of charge concentration between the sulfur and doubly-bonded groups is more spread out in this plane than in the axial plane shown in Figure 4. The increase in the region of space occupied by the doubly-bonded charge concentration in the equatorial plane on going from Y = O to Y = CH_2 is also clear in these plots.

Oberhammer and Boggs[10] have commented that the increase in the F_{eq}–S–F_{eq} angle by 10° on replacing the lone pair in SF_4 by the double bond in OSF_4 and the decrease in this angle by 4° on replacing it by the double bond in H_2CSF_4 are not in accord with the VSEPR model. Shortly after, however, Christe and Oberhammer[12] pointed out that the bond angles in OSF_4 and H_2CSF_4 could be rationalized if the relative populations of the π_{eq} and π_{ax} components of the S–X double bonds are taken into

(12) Christe, K. O.; Oberhammer, H. *Inorg. Chem.* **1981**, *20*, 296.

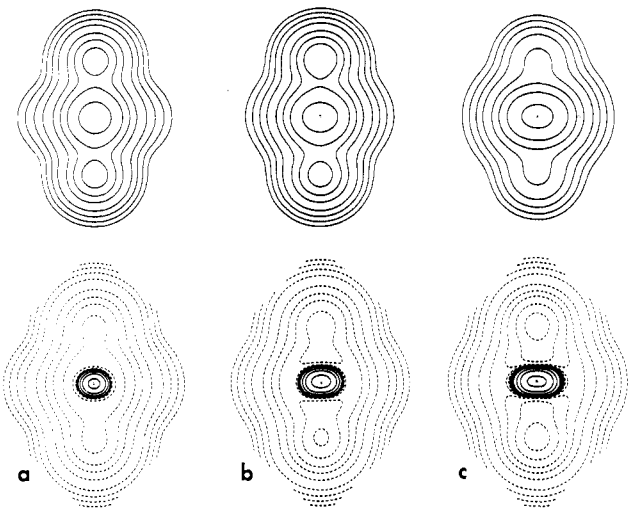

Figure 6. Contour maps of ρ (top) and $\nabla^2\rho$ (bottom) for the SF_4Y molecules analogous to those shown in Figure 3: (a) OSF_4; (b) $HNSF_4$; (c) H_2CSF_4. These plots are viewed in the plane obtained by taking a vertical slice through the bond critical point (for the plot of ρ) and through the nonbonded charge concentration maximum (for the plot of $\nabla^2\rho$). These plots show the manner in which the doubly-bonded charge concentration is spread out in the equatorial plane and illustrates the values of ϵ_L given in Table 3.

Table 4. Calculated and Observed S–Y Bond Lengths (pm)

	H_2CSF_4	$HNSF_4$	OSF_4
obsd	156	146[a]	141
calcd[b]	156	147	140
sum of double-bond radii[c]	161	154	146
sum of single-bond radii[c]	181	174	166

[a] Calculated value from ref 11. [b] This work. [c] Reference 12.

account. The *ab initio* molecular orbital calculations performed by Oberhammer and Boggs[10] gave populations of $\pi_{eq} = 0.17$ au and $\pi_{ax} = 0.12$ au for OSF_4 and $\pi_{eq} = 0.23$ au and $\pi_{ax} = 0.02$ au for H_2CSF_4. These results indicate that the C–S double bond exerts a much greater repulsive effect in the equatorial plane than the O–S double bond and hence leads to a smaller F_{eq}–S–F_{eq} angle in H_2CSF_4 than in OSF_4.

Our results, which show that the cross section of the electron density in these double bonds is elliptical and that it is considerably more elliptical in the C–S than in the O–S bond, provide an alternative description of these bonds that confirms this earlier suggestion—described in terms of the σ–π model. In H_2CSF_4 the electron density of the C–S bond is forced very much into the equatorial plane, resulting in a small F_{eq}–S–F_{eq} bond angle. The lone pair of SF_4 is not constrained in shape like the C–S double bond but spreads into the equatorial plane, where there is more space available for it than in the axial plane, although it is less confined to the equatorial plane than the C–S double bond, giving a larger F_{eq}–S–F_{eq} angle. In contrast, the S–O double bond is not confined to the equatorial plane by any other bonds formed by the oxygen atom and is much more symmetric. This bond has relatively less charge density in the equatorial plane and more in the axial plane, so that the F_{eq}–S–F_{eq} angle is larger than it is in SF_4.

The Nature of the S–Y Bond. The conventional Lewis diagrams (structural formulas) for the molecules H_2CSF_4, $HNSF_4$, and OSF_4 are usually drawn with an S–Y double bond. The formulation of these bonds as double bonds is in accord with (1) experimental bond lengths, (2) electron density at the bond critical point, and (3) the ellipticities of the C–S and N–S bonds in H_2CSF_4 and $HNSF_4$ and the geometry around the C and N atoms in these molecules.

(1) The S–Y bond lengths given in Table 4 are much shorter than the lengths calculated from single-bond radii and are close to those calculated from double-bond radii.[13] They are also much shorter than the observed S–OH bond length in H_2SO_4 (Table 5).

Table 5. Various Observed[a] and Calculated Properties for Bonds in SO_2X_2 (X = OH, F) Molecules[b]

	$SO_2(OH)_2$	SO_2F_2
r(S=O)/pm	140.2	138.6
	[142.2]	[139.7]
ϵ_ρ	0.006	0.040
ρ	0.331	0.342
$\nabla^2\rho$	–0.954	–0.975
r(S—X)/pm	156.2	152.4
	[157.4]	[153.0]
ϵ_ρ	0.022	0.057
ρ	0.241	0.222
$\nabla^2\rho$	–0.624	–0.259
∠O=S=O/deg	123.5	125.1
	[123.3]	[122.6]
∠X—S—X/deg	101.9	95.5
	[101.3]	[96.7]

[a] Hargittai, I. *The Structure of Volatile Sulfur Compounds*; D. Reidel: Dordrecht, The Netherlands, 1985. [b] Geometric parameters were obtained from an optimization at the HF6-311G** level of theory, and values of $\nabla^2\rho$ given are for the charge concentration along the bond. Observed bond lengths and angles are shown in brackets underneath the calculated values.

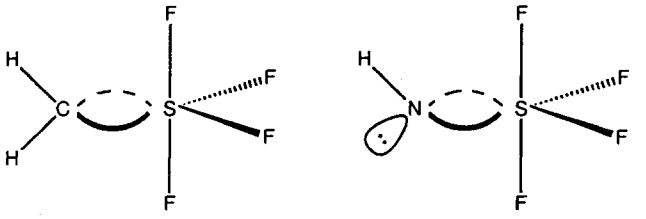

Figure 7. Bent-bond model of the H_2CSF_4 molecule.

(2) From the data in Tables 3 and 5 we can compare the electron density of the S–O bond of SOF_4 at the bond critical point with that of the S–O bonds in SO_2F_2 and $SO_2(OH)_2$. We see that these electron densities are very similar for all the bonds described as S=O double bonds in the conventional Lewis structure and are considerably greater than the electron densities in the formally single S—OH and S—F bonds.

(3) The ellipticities of the electron density of the S–X bond and of the Laplacian of the bonding charge concentration for H_2CSF_4 and $HNSF_4$ given in Table 3 show that the electron density in the S–X bond is greater in the equatorial plane than in the axial plane. These bonds may be described in terms of the σ–π model with the π-bond in the equatorial plane or in terms of the "bent-bond" model. The bent-bond model is based on an octahedral arrangement of six electron pairs around the sulfur atom and a tetrahedral arrangement of four electron pairs around the X atom, with two pairs forming a double bond (Figure 7). The bent-bond model predicts clearly that the N–H bond and the C–H bonds should lie in the axial plane of the $HNSF_4$ and H_2CSF_4 molecules, as observed.

Laplacian of the Charge Concentration and the VSEPR Model. In previous work it has been shown that for many molecules there is a direct correspondence between the number and geometrical arrangement of valence shell electron-pair domains, as predicted by the VSEPR model, and the number and geometrical arrangement of the valence shell charge concentrations (VSCC's) found in the Laplacian of the electron density.[3,4] However, for some fluorides bonding charge concentrations are not observed in the valence shell of the central atom although a nonbonded charge concentration is found in the same molecules.[14]

(13) (a) Pauling, L. *Nature of the Chemical Bond*, 3rd ed.; Cornell University Press: Ithaca, NY, 1960. (b) Gillespie, R. J.; Robinson, E. A. *Inorg. Chem.* **1992**, *31*, 1960.

(14) Bytheway, I.; Gillespie, R. J.; Bader, R. F. W. Unpublished results.

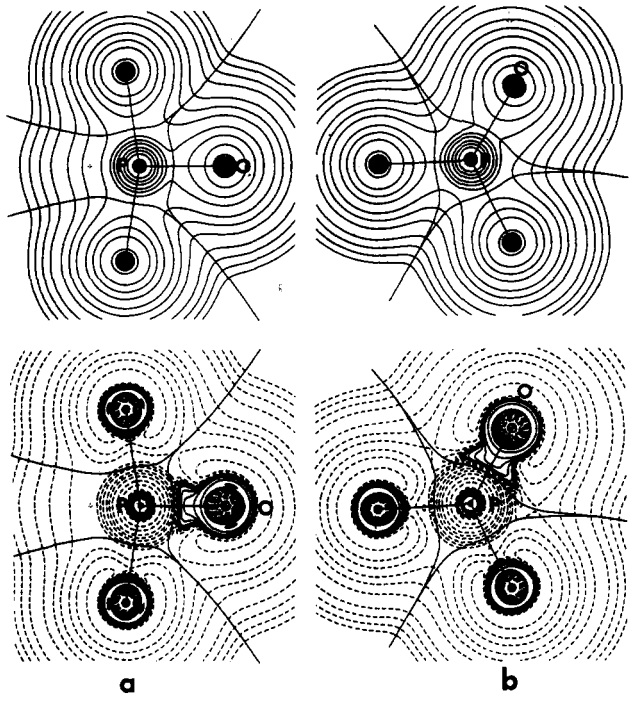

Figure 8. Contour maps of ρ (top) and $\nabla^2\rho$ (bottom) for the OPF_4^- molecule: (a) viewed in the plane containing the axial fluorine, central phosphorus, and oxygen atoms; (b) viewed in the plane containing the equatorial fluorine, central phosphorus, and oxygen atoms. In both views the lack of charge concentration maxima between the phosphorus and fluorine atoms is evident, and although a region of charge concentration between the phosphorus and oxygen atoms exists, there is no local maximum in this region.

We noted above the absence of bonding charge concentrations in PF_4^-, and we have also studied OPF_4^-, which has the expected trigonal bipyramidal geometry with the double bond in an equatorial position, as in the isoelectronic OSF_4. Figure 8 shows no bonding charge concentration along either the P–F or P–O bond. We have found that bonding charge concentrations are similarly absent in molecules such as CaF_2, which are considered to be very ionic, *i.e.*, in which there is considerable charge transfer to the fluorine atoms.[14] This charge transfer depletes the electron density in the bonding regions to such an extent that the valence shell charge concentrations are no longer observed. The absence of bonding charge concentrations does not, however, imply the absence of a bond but implies only that the bonds are rather ionic (polar). That bonds exist is demonstrated by the presence of a bond critical point in the charge density between the phosphorus and fluorine and between the phosphorus and oxygen atoms. Table 6 shows that the values of ρ at the bond critical points in these molecules are, however, smaller than in molecules for which bonding VSCC's are observed. It would appear that no bonded VSCC is observed when ρ at the bond critical point is less than about 0.18 for A–F bonds and less than about 0.27 for A–O bonds.

Table 6. Values of the Charge on Fluorine and ρ and $\nabla^2\rho$ at Bond Critical Points for Various Fluorine-Containing Molecules

bond type	molecule	ρ	$\nabla^2\rho$	$-q$(F)	bonding VSCC	ref
Na–F	NaF	0.0519	0.442	0.900	no	*a*
Mg–F	MgF_2	0.0730	0.738	0.880	no	*a*
K–F	KF	0.0495	0.267	0.930	no	*a*
Ca–F	CaF_2	0.0765	0.466	0.893	no	*a*
P–F_{ax}	PF_4^-	0.119	0.273	0.865	no	*b*
P–F_{eq}		0.148	0.797	0.845	no	
P–F	OPF_3	0.183	1.298	0.810	no	*a*
P–F_{ax}	OPF_4^-	0.136	0.666	0.852	no	*b*
P–F_{eq}		0.156	0.933	0.836	no	
Cl–F	$ClF_2O_2^-$	0.125	0.266	0.702	no	*a*
Cl–F_{ax}	ClF_4^+	0.257	−0.409	0.426	yes	*b*
Cl–F_{eq}		0.297	−0.781	0.309	yes	
N–F	ONF_3	0.377	−0.743	0.305	yes	*a*
S–F_{ax}	SF_4	0.180	0.125	0.708	yes	*b*
S–F_{eq}		0.220	0.545	0.696	yes	
S–F_{ax}	OSF_4	0.205	0.311	0.713	yes	*b*
S–F_{eq}		0.227	0.593	0.695	yes	
S–F_{ax}	$HNSF_4$	0.190	0.179	0.717	yes	*b*
S–F_{eq}		0.222	0.537	0.718	yes	
S–F_{ax}	H_2CSF_4	0.195	0.337	0.750	yes	*b*
S–F_{eq}		0.215	0.455	0.732	yes	

[a] Reference 14. [b] This work.

Conclusions

The location, size, and shape of the valence shell charge concentrations in the laplacian of the electron density of the molecules that we have studied confirm and extend the predictions of the VSEPR model. For many purposes we can equate the VSCC's in the Laplacian of the electron density to the electron-pair domains of the VSEPR model. Thus, except for very ionic bonds, the number, location, size, and shape of the VSCC's correspond closely to the number, location, size, and shape of the electron-pair domains of the VSEPR model. In particular, the elliptical shape of both nonbonding and double-bond VSCC's confirms assumptions that must be made about the size and shape of the VSEPR electron-pair domains of lone pairs and double bonds in order to account for otherwise apparently anomalous bond angles.

This work is a continuation of attempts to understand the physical basis of the VSEPR model and to understand both its successes and failures. It is evident from the present work that the basic tenet of the VSEPR model, that molecular shape is governed by interactions between bonded and nonbonded electron-pair domains (localized charge concentrations), is valid. The relative sizes and shapes of the regions of charge concentration, as revealed in the laplacian of the charge density must, however, be taken into account if the details of the geometry of some molecules are to be understood.

Acknowledgment. Financial support from the Natural Sciences and Engineering Council of Canada is gratefully acknowledged. We also thank Dr. K. Christe for communication of results prior to publication.